System Identification of an S500 Quadrotor UAV

Judson T. Babcock *
Department of Aeronautics, U.S. Air Force Academy, Colorado, 80841

The S500 is a kit-built quad-rotor aircraft measuring 500 mm diagonally from motor to motor and weighs 3 pounds with a 3-cell 5200 mAh battery installed. The aircraft is flight tested to obtain longitudinal and lateral-directional models of the bare airframe using frequency-response system identification. Frequency sweeps are flown in longitudinal, lateral, collective, and pedal inputs in the stabilize flight mode of PX4 autopilot. The frequency responses are used to identify the longitudinal and lateral-directional state-space models of the vehicle in hover with the cost functions, Cramér-Rao bounds, and insensitivity of both models within acceptably low bounds. The models reveal an unstable oscillatory mode in longitudinal and lateral-directional motion, as is typical for rotorcraft in hover. The models show good agreement with the frequency data and time-domain doublet data and are suitable for future control development on the S500 quad-rotor.

I. Nomenclature

a_x, a_y, a_z	x, y, z accelerations, m/s/s	T_{rec}	Record length, s
a_0, a_1	Transfer function coefficients	T_{max}	Maximum period, s
g	Acceleration due to gravity, m/s/s	u, v, w	Aircraft x, y, z velocities, m/s
J	Cost function	$\delta_{a,e}$	Aileron, elevator deflection, deg
k	Gain	$\delta_{left,right}$	Elevon deflection, deg
$L_p, L_r, L_v, L_{\delta_{lat}}$	Rolling moment stability parameters	δ_{col}	Throttle input, %
$M_q, M_u, M_w, M_{\delta_{lon}}, M_{\delta_{col}}$	Pitching moment stability parameters	ϕ	Bank angle, deg
N	Scale factor	θ	Pitch angle, deg
$N_p, N_r, N_v, N_{\delta_{lat}}$	Yawing moment stability parameters	τ_c	Time constant, s
$X_q, X_u, X_w, X_{\delta_{lon}}, X_{\delta_{col}}$	X-force stability parameters	τ_δ	Time delay of control input, s
$Y_p, Y_r, Y_v, Y_{\delta_{lat}}$	Y-force stability parameters	ω	Frequency, rad/s
$Z_q, Z_u, Z_w, Z_{\delta_{lon}}, Z_{\delta_{col}}$	Z-force stability parameters	ζ	Damping ratio
p, q, r	Roll, pitch, and yaw rates, deg/s		

*Lieutenant Colonel and Assistant Professor, USAFA-DFAN, 2140 Faculty Drive, USAFA, CO 80840, AIAA member

II. Introduction

The S500 quad-rotor is a generic, flexible platform which can be used for surveillance, photography, package delivery, payload support, or personal entertainment. The availability of commercial components and open-source software has made platforms like the S500 very popular due to their ability to be easily scaled, reconfigured, and operated. However, fine-tuned or advanced flight control is usually not achieved for the same reasons: rapid changes in aircraft dimensions, components, or mission parameters usually require re-tuning control laws for each configuration. Instead, most commercially available UAS platforms use generic PID controls laws with simple gain tuning, which is sufficient for most purposes. To achieve more advanced flight control, modeling and simulation of each particular vehicle configuration is required, making the endeavor intractable for most commercial UAS manufacturers or do-it-yourself kits.

A. Background

Multi-rotor vehicles are preferred among many users for their ability to hover and loiter while providing a flexible platform for various sensors or mission payloads. Their ability to takeoff and land from almost any location is another key advantage they provide.

Due to the inherent dynamic instabilities of rotorcraft, multi-rotor vehicles must be flown with a closed-loop autopilot to provide stabilization and tracking of pilot commands. Popular open-source autopilot software includes ArduPilot and PX4. Both platforms support a wide variety of vehicle configurations including multi-copter and fixed-wing vehicles and both provide a variety of flight modes such as position hold, altitude hold, stabilization, and more.

Control law design and tuning requires an accurate model of the vehicle under consideration. Simulation of the mathematical model allows for benchtop tuning of the control loops before flight testing. Although the control design process is an iterative process, obtaining an accurate and verified model of the aircraft is a critical step to ensure that the control law can be tuned before flight using a simulation which accurately represents the vehicle in flight.

System identification extracts a real-world model of the vehicle dynamics by measuring and recording the dynamic response to known control inputs during a flight test experiment. The specified control inputs in each axis excite the aircraft motion while the aicraft responses are recorded. The system identification process applies to any system or subsystem that has a predictable input-output relationship. The frequency-response approach to system identification has been shown to be an accurate, reliable method for obtaining accurate models of aircraft and rotorcraft [1–4]. The software package CIFER® (Comprehensive Identification from Frequency Responses) makes these proven techniques available in a robust and systematic way, allowing the engineer to process, obtain, and validate flight dynamic models for a wide range of aircraft or rotorcraft [5].

B. Theory

The system identification process follows a logical progression from obtaining flight data to verification of the resulting model. The process implemented in CIFER® is shown in Fig. 1 [5] and begins with the flight test experiment using the final aircraft configuration in a representative, real-world environment. During the experiment, the pilot creates an oscillating input in each axis which varies in frequency over the duration of the input. This frequency sweep begins with the maximum period of oscillation required as determined from the minimum dynamic frequency of the expected dynamic modes, as shown in Eq. (1). The pilot's inputs should oscillate around trim as they are increased in frequency, producing a total record length for the input which is 4-5 times longer than the maximum period of interest and ending at a frequency higher than the maximum expected frequency of the relevant dynamic modes of the aircraft. For a rotorcraft, this procedure must be repeated in each input: the lateral cyclic input (δ_{lat}) for roll, the longitudinal cyclic input (δ_{lon}) for pitch, the pedal input (δ_{ped}) for yaw, and the collective input (δ_{col}) for vertical acceleration.

$$T_{max} = \frac{2\pi}{\omega_{min}} \tag{1}$$

The measured flight data must then be examined to identify and correct any measurement errors such as drift, bias, or mis-alignments in time. Depending on the severity of the errors, the flight experiment may need to be repeated. Verification of angular, translational, and kinematic consistency can help identify errors in the experimental setup. Because the aircraft motion is being measured in a non-inertial reference frame, the translational accerelations ($\dot{u}, \dot{v}, \dot{w}$) as observed in the inertial reference frame must be reconstructed from the body angular rates (p, q, r), the specific external forces recorded by the accelerometers (a_x, a_y, a_z), and the trim conditions ($U_0, V_0, W_0, \theta_0, \phi_0$).

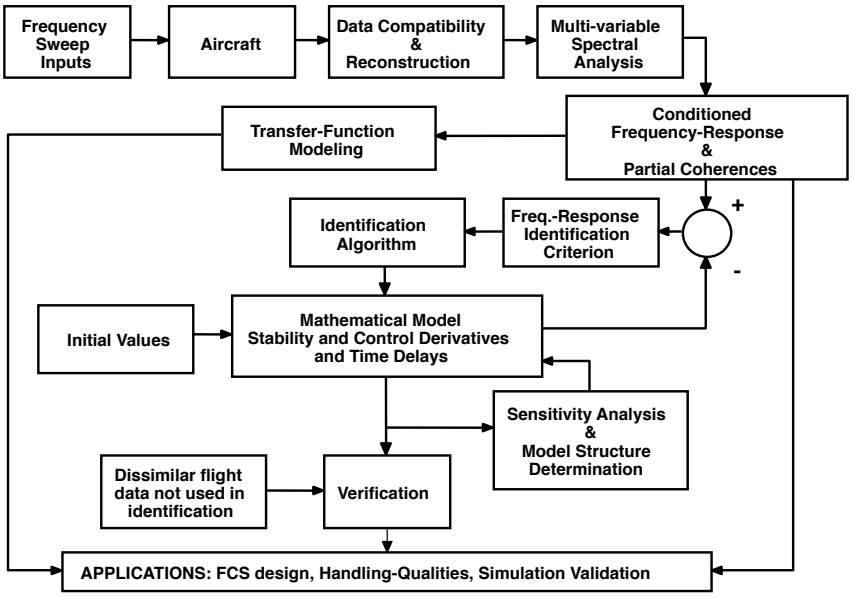

Fig. 1 CIFER® frequency-response method for system identification [5]

The resulting time-domain data is analyzed as a function of frequency using spectral analysis with a chirp-z transform and half-sine overlapping windows to reduce noise. Five separate windows and their corresponding sizes are chosen to best reduce noise in the frequency range of interest, allowing the spectral results to be optimized together into a composite frequency response for each particular input. The chirp-z and optimal window techniques greatly improve the quality of the frequency response as compared to a traditional FFT. For flight maneuvers with correlated secondary inputs, an additional procedure is used to isolate the input-output effect of the primary control surface. The spectral analysis process also quantifies the coherence at each frequency, which indicates the amount of output that is dependent on the input at that frequency [5].

Parametric transfer function models can be obtained next using a pole-zero description of the system response to an input. After choosing the order of the transfer function model, a numerical, coherence-weighted algorithm optimizes the values of the numerator and denominator coefficients to minimize the magnitude and phase errors between the model and the frequency response data, resulting in a cost function J. An equivalent time delay accounts for phase lag from higher-order modes or transport delays within the system.

A state space model can then be identified from the resulting frequency responses to characterize the response of a multiple-input multiple-output (MIMO) systems. First, the user specifies the a model structure to capture each frequency response of the flight data in the MIMO model. A cost function is used to quantify the fit of the model, both for each individual frequency response contained in the model and the overall model. Each parameter is identified using a pattern-search method which starts with user-specified initial values. While each parameter is varied, the cost function is calculated to find the solution which minimizes the average cost function (J_{avg}) of the complete system within the available frequency range of the data. Each resulting parameter is assessed for its standard deviation (using the Cramér-Rao inequality) and sensitivity. This allows the user to estimate the uncertainty in each parameter and eliminate them from the model as needed. Insensitive parameters are those which have no discernable effect on the average cost function and are also removed from the model.

Finally, the state space model is verified using the transfer functions of the measured flight data and using time domain data with dissimilar flight manuevers. The equations of motion (with the identified parameters) can be integrated in time using the control inputs from the maneuver, such as a doublet, along with estimates for the trimmed reference shifts of the aircraft before the maneuver. Good agreement between the model and the flight data in the time domain confirms the predictive capability and usefulness of the model.

C. Prior Work

Mettler et al. [6] used the frequency response approach to successfully model the flight dynamics of a large model

helicopter with a 10-ft diameter rotor, concluding that the system identification technique was valid with that size vehicle if the proper instrumentation is present. Results showed an unstable eigenvalue pair corresponding to a phugoid-type horizontal motion with the other modes being stable.

Lederbogen et al. [3] applied the technique to a smaller helicopter with a 4-ft diameter rotor, achieving good modeling results for transfer functions in each axis. Excellent results were also obtained for the 6DOF state space model, with stable eigenvalues in hover. In forward flight, the identified 6DOF model showed a better results without any coupling terms included and resulted in one unstable real eigenvalue. Overall, the location of the instrumentation below the center of gravity was highlighted as a concern.

Cai et al. [7] used a small quad-rotor in an effort to identify the model parameters in hover in closed-loop stabilized flight over a frequency range from about 2-26 rad/s, with good matching in the frequency and time domain between the flight data and the model.

Wei et al. [8] identified a closed-loop dynamic model of an approximately 2-ft diameter quad-rotor vehicle over a frequency range of 0.3-35 rad/s. The linear model was an adequate representation of the flight vehicle with stable eigenvalues and compared favorably to the actual flight data used for verification.

On a smaller scale quad-rotor platform with a 13 inch diagonal dimension, Niermeyer et al. [9] identified separate state space models for the pitch/roll response, yaw response, and vertical response. Because the identified open loop model was unstable, it was validated through a closed-loop simulation using the same PI controller on the flight vehicle.

Navarro et al. [10] modeled a quad-rotor with an 2-foot diagonal size from motor to motor, with dual counter-rotating motors on each corner for a total of eight propellers. The system used a Pixhawk PX4 autopilot. The authors identified model parameters from individual transfer function fits with good comparisons between the transfer functions and the flight data in the frequency and time domains. Cho et al. [4] extended the work on a vehicle with the same coaxial configuration but slightly smaller size, obtaining transfer functions and a state space model which contained a coupled model structure with additional states added to account for motor lag and lag in the yaw dynamics. The model was accurate in a frequency range of 0.5-60 rad/s. The model showed unstable dynamic modes in both longitundal and lateral directions, similar to Cheung et al. [11]. The authors extended the work to design and deploy an optimized control law on the vehicle, achieving good results with reduced actuator usage.

Yuksek et al. [12] used a faster, agile racing quad-rotor as the basis for their work with frequency sweeps designed to cover 1-60 rad/s in hover and forward flight. They used a separate estimation procedure using transfer functions for the difficult speed damping and speed stability derivatives which improved their model fit, and verified the model over short time periods to avoid difficulties with simulating the unstable bare airframe model.

D. Objectives

A verified flight dynamic model of the S500 quadrotor is desired to allow for follow-on control law tuning and deployment on the vehicle. The frequency-response identification procedure will be performed on flight data obtained from piloted sweeps in the longitudinal, collective, lateral, and pedal inputs. The model will be verified against doublets performed in manual mode in each axis to determine the accuracy and usefulness of the models for future flight control development.

III. Methods

Flight test experiments are designed and conducted on the S500 quadroter in order to obtain the required frequency response data using each flight control input. Multiple flights over multiple days were accomplished to gather the necessary data of sufficient quality for the identification procedure.

A. Flight Vehicle

The S500, depicted in Fig. 2, measures 500mm diagonally from motor to motor and weighs 3 lbs with the battery installed underneath the vehicle. It is powered by 2216-920 kV motors with 1045 propellers and is flown using a Pixhawk 4 autopilot with PX4 firmware version XXX. A M8N GPS module with compass provides position and direction information while a SiK 915 MHz 100 mW radio provides telemetry to the ground station. Piloted flight is achieved with a Jeti hand controller which is capable of switching between flight modes. A flight time of approximately 10 minutes is possible with the 3-cell 5200 mAh LiPo battery.

Fig. 2 S500 Quadrotor UAS

B. Experimental Setup

Flights are accomplished in an open-air park using the hand controller with the vehicle starting in hover. The PX4 stabilize flight mode is used which provides basic stabilization for the naturally unstable airframe. In the stabilize flight mode, the pilots roll/pitch inputs command a tilt angle, the yaw inputs command a yaw rate, and the throttle commands rate of ascent or descent. The aircraft takes off vertically, receiving inputs from the pilot via the radio controller while reporting its position, airspeed, and altitude to the ground station which consists of a laptop running QGroundControl.

C. Procedures

After many preliminary training flights, a final series of three flights were conducted to obtain the necessary data. The first flight lasted for approximately 8 minutes conducted the frequency sweeps shown in Table 1. The second flight also lasted for eight minutes, resulting in 13 sweeps across the four flight inputs with record lengths ranging from 18 to 26 seconds.

Table 1 Test Matrix

Flight	Input	# Sweeps	Avg T_{rec} [s]
1	δ_{lon}	5	21.2
1	δ_{col}	1	25.5
2	δ_{lat}	4	19.2
2	δ_{ped}	3	22.1
2	δ_{col}	4	20.2
3	all	doublets	-

For each sweep, the pilot focused on starting in hover, conducting two long period oscillations, then slowly increasing the frequency of the input until achieving the fastest input possible, and finally ending back in trim. Example sweeps are shown in Fig. 3, showing the smooth progression in frequency and the roughly symmetric oscillations about trim.

After each flight, the data are examined to find the starting and ending time of each sweep. Then the data from the various flight sensors are synchronized to a common 200 Hz time step and the individual sweeps are exported for use in CIFER®. The input signal for the system identification procedure is taken from the outputs of the flight controller sent to the onboard mixer in order to obtain a bare airframe model without the controller dynamics included.

Spectral analysis is conducted next using the window and frequency ranges shown in Table 2, which were chosen to conform to best practices for window lengths [5]. The results from all windows are optimized together to create a composite frequency response for each input, and any correlated secondary inputs are removed from the primary input's frequency response.

A longitudinal state space model is identified using the state equation shown in Eq. (2), where q, u, w, θ are the states, $\delta_{lon}, \delta_{col}$ are the control inputs, $\tau_{\delta_{lon}}, \tau_{\delta_{col}}$ are the time delays, U_0, W_0, θ_0 are trim values which are zero in

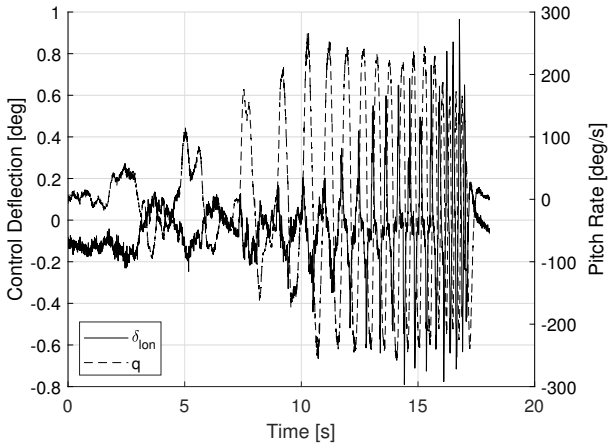

(a) Longitudnal input

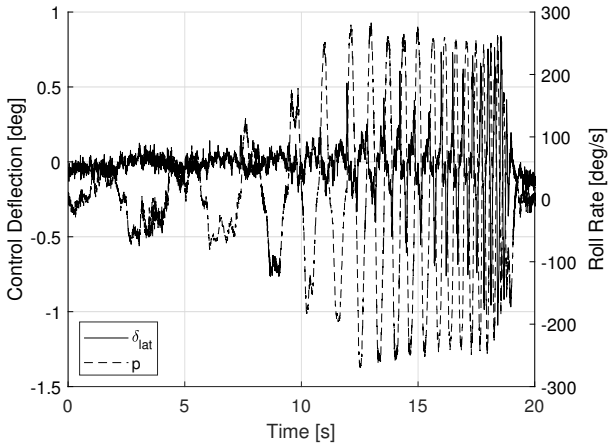

(b) Lateral input

Fig. 3 Time history of selected sweeps showing angular rate responses

Table 2 Window lengths and frequency ranges for spectral analysis

Input	# Sweeps	Min T_{win} [s]	Max T_{win} [s]	ω_{min} [rad/s]	ω_{max} [rad/s]
δ_{lon}	5	5.0	9.0	0.70	30
δ_{col}	5	3.8	8.9	0.70	30
δ_{lat}	4	6.0	14.0	0.45	10
δ_{ped}	3	6.0	14.0	0.45	10

hover, and the stability parameters are represented by $M_q, M_u, M_w, M_{\delta_{lon}}, M_{\delta_{col}}$, etc. The input parameters $M_{\delta_{col}}$ and $X_{\delta_{col}}$ were found to be negligible through the data reduction process and were removed from the model. The outputs, not shown, include the states and the accelerations a_x and a_z.

$$\begin{bmatrix}\dot{q}\\ \dot{u}\\ \dot{w}\\ \dot{\theta}\end{bmatrix} = \begin{bmatrix} M_q & M_u & M_w & 0 \\ X_q - W_0 & X_u & X_w & -g\cos\theta_0 \\ Z_q + U_0 & Z_u & Z_w & -g\sin\theta_0 \\ 1 & 0 & 0 & 0 \end{bmatrix}\begin{bmatrix}q\\ u\\ w\\ \theta\end{bmatrix} + \begin{bmatrix} M_{\delta_{lon}} & M_{\delta_{col}} \\ X_{\delta_{lon}} & X_{\delta_{col}} \\ Z_{\delta_{lon}} & Z_{\delta_{col}} \\ 0 & 0 \end{bmatrix}\begin{bmatrix}\delta_{lon}\\ \delta_{col}\end{bmatrix}\begin{bmatrix}t-\tau_{\delta_{lon}}\\ t-\tau_{\delta_{col}}\end{bmatrix} \tag{2}$$

The same form is followed for the lateral-directional model shown in Eq. (3), where p, r, v, ϕ are the states, δ_{lat} and δ_{ped} are the inputs, and the stability parameters are represented, for example, by $L_p, L_r, L_v, L_{\delta_{lat}}$. The output equation, not shown, includes a_y in addition to the states.

$$\begin{bmatrix}\dot{p}\\ \dot{r}\\ \dot{v}\\ \dot{\phi}\end{bmatrix} = \begin{bmatrix} L_p & L_r & L_v & 0 \\ N_p & N_r & N_v & 0 \\ Y_p + W_0 & Y_r - U_0 & Y_v & g\cos\theta_0 \\ 1 & 0 & 0 & 0 \end{bmatrix}\begin{bmatrix}p\\ r\\ v\\ \phi\end{bmatrix} + \begin{bmatrix} L_{\delta_{lat}} & L_{\delta_{ped}} \\ N_{\delta_{lat}} & N_{\delta_{ped}} \\ Y_{\delta_{lat}} & Y_{\delta_{ped}} \\ 0 & 0 \end{bmatrix}\begin{bmatrix}\delta_{lat}\\ \delta_{ped}\end{bmatrix}\begin{bmatrix}t-\tau_{\delta_{lat}}\\ t-\tau_{\delta_{ped}}\end{bmatrix} \tag{3}$$

Frequency ranges for each input-output pair in the models are chosen based on a coherence cutoff criteria of 0.4 while avoiding regions with significant oscillation in coherence. Each model is initially converged and the average cost function J_{avg} is examined along with the individual cost functions of each input-output pair. A cost function below 100 is considered acceptable and below 50 is desirable. The eigenvalues of the model are also examined to assess the characteristic motion and overall realism of the model. The model is reduced to remove any insensitive parameters or parameters with large standard deviations as indicated by the Cramér Rao percentage. Parameters are removed one at a time, starting with the highest insensitivity or Cramér Rao percentage, and the model is re-converged each time to

recheck the cost function, eigenvalues, insensitivities, and Cramér Rao bounds. This procedure is followed until there are no parameters remaining with high insensitivity or Cramér Rao bounds or until the average cost function jumps by more than 2, which indicates a drop in model accuracy.

Finally, the model is verified in the time domain against doublet flight maneuvers in each axis. A separate identification procedure identifies the residual errors in the trim condition, including process noise such as turbulence, as well as the reference shifts for each motion output [5]. A dimensional cost function, J_{rms}, results from this procedure, where values below 1-2 indicate an acceptable level of accuracy for a full scale aircraft. For a small scale aircraft, this cost function guideline must be Froude scaled by $\sqrt{N}$, where N is a scale factor based on the ratio of the model wingspan to full scale (e.g., $N = 5$ refers to 1/5th of full scale) [6]. Compating the S500 diameter to a full-scale helicopter rotor diameter, $N \approx 16$, and the acceptable range of cost function values becomes 16-32. After identifying these offsets for each maneuver, the control inputs from the maneuver are input into the model which is integrated over time. The output from the model is compared to the flight data from that maneuver to determine if the model adequately predicted the aircraft's motion as recorded by the onboard sensors.

IV. Results and Discussion

Composite frequency responses for q/δ_{lon}, A_z/δ_{col}, p/δ_{lat}, and r/δ_{ped} are shown in Fig. 4. Coherence for q/δ_{lon} begins low but is strong in the range of 3-45 rad/s, above which it begins to oscillate which is a sign of decreased quality in the frequency response. For A_x/δ_{col}, the coherence is smooth and acceptable up to 21 rad/s, above which it begins to drop and oscillate.

In the lateral responses, coherence for p/δ_{lat} begins low but is acceptable strong and smooth between the frequency range of 4-30 rad/s. The frequency response for r/δ_{ped} shows a good result in the range of 1-21 rad/s. Overall, all responses are strong and useful for the purpose of system identification.

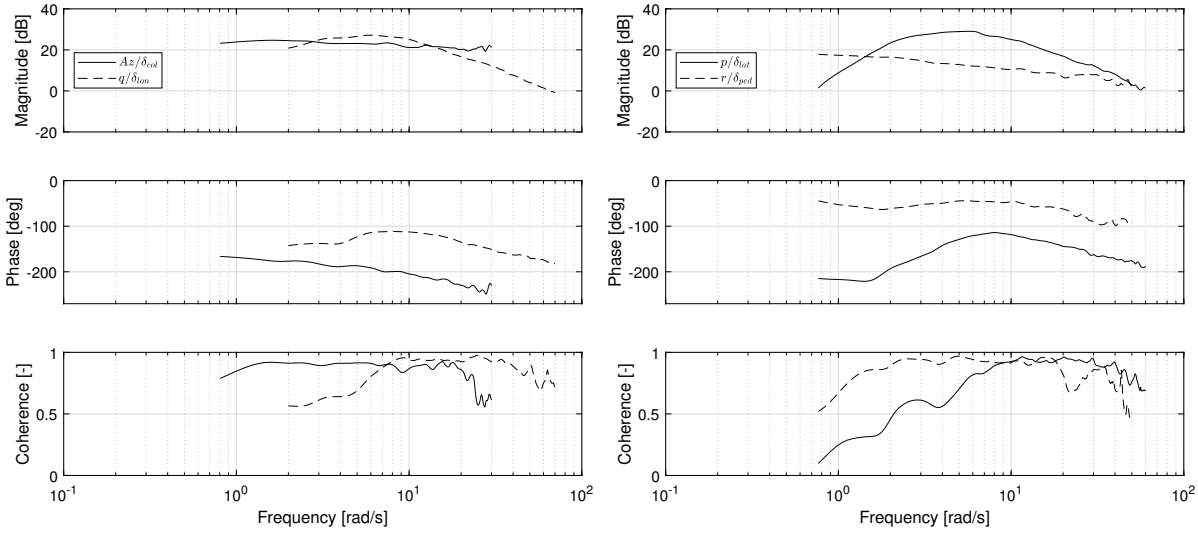

(a) Longitudinal mode (b) Lateral mode

Fig. 4 Primary on-axis frequency responses in longitudinal and lateral directions

A. Longitudinal Model

To aid the identification of the longitudinal state-space model at low frequencies, the speed-damping derivative X_u is identified using a transfer function fit to $\dot{u}/\theta(s)$ as seen in Eq. (5) [5, 12]. A frequency range of 2-13 rad/s was chosen based on the coherence in the flight data. The resulting value of X_u is -0.25/s.

$$\dot{u}/\theta(s) = \frac{-sg}{s - X_u} \tag{4}$$

The longitudinal state space model is identified using the frequency response pairs and ranges shown in Table 3. The acceptable frequencies vary but most responses have a spread of 10-40 rad/s. The individual (J) and average (J_{avg}) cost functions of the final model are also shown, with the average cost functions of 26.5 being well under the guideline of 50, indicating a model that matches the flight data very closely.

Table 3 Longitudinal model frequency range and cost functions

Response	ω_{min} [rad/s]	ω_{max} [rad/s]	J [-]
q/δ_{lon}	3.0	45	54.2
A_x/δ_{lon}	5.0	35	29.6
A_z/δ_{lon}	9.0	20	21.1
$\dot{u}/\delta_{lon}$	2.1	11	30.0
A_z/δ_{col}	0.81	21	12.2
$\dot{w}/\delta_{col}$	0.81	21	17.7
J_{avg} [-]			26.5

The resulting model parameters, Cramér-Rao bounds, and insensitivities are listed in Table 4. The X_w and Z_q parameters are dropped from the model during the model reduction due to high insensitivity and poor Cramér-Rao bounds, and the X_u parameter reflect the value found through the transfer function procedure. Insensitivity and Cramér-Rao bounds remained high on M_q and X_q, but the parameters were retained because the cost function jumped significantly without them. Additional longitudinal sweeps, or longer sweeps, may help improve the confidence in these parameters. The other identified parameters have very low insensitivity. The longidutinal and collective time delays are very similar, around 40 ms, which is expected since the drone uses the same motor throughout.

The model eigenvalues are shown in Table 5 and display the characteristic modes for a rotorcraft in hover. The vehicle is unstable in hover, as expected, which is characterized by a pair of unstable oscillatory eigenvalues. Stable first order modes characterize the vertical motion of the aircraft.

Table 4 Identified longitudinal model parameters

Parameter	Value	Cramér-Rao [%]	Insensitivity [%]
M_q [1/s]	0.9	54.6	14.6
M_u [1/s]	10.8	13.7	2.1
M_w [1/s]	26.6	28.2	2.5
X_q [1/s]	-0.08051	32.1	13.38
X_u [1/s]	-0.25	-	-
X_w [1/s]	-	-	-
Z_q [1/s]	-	-	-
Z_u [1/s]	0.3558	48.6	2.926
Z_w [1/s]	0.7	47.8	3.8
$M_{\delta_{lon}}$ [1/s^2]	149.8	3.1	1.3
$X_{\delta_{lon}}$ [m/s^2]	-7.2	4.0	1.9
$Z_{\delta_{lon}}$ [m/s^2]	-5.7	4.2	2.1
$Z_{\delta_{col}}$ [m/s^2]	-13.8	3.7	1.4
$\tau_{\delta_{lon}}$ [s]	0.037	4.8	2.0
$\tau_{\delta_{col}}$ [s]	0.039	10.9	4.7

Verification of the stable longitudinal motion is shown in Fig. 5 in response to collective and longitudinal inputs.

Table 5 Longitudinal eigenvalues of the S500 quad-rotor

Mode	Real	Imaginary	ζ [-]	ω_n [rad/s]
1	-0.19	0.00	–	–
2	-3.81	0.00	–	–
3	2.66	± 3.82	-0.57	4.65

The model tracks the vertical acceleration closely. Verification of the unstable modes is analyzed in the frequency domain using a transfer function comparison to the flight data. As shown in Fig. 6, the frequency response for horizontal acceleration and pitch rate from the model matches the flight data very closely with high coherence across the frequency range. The model differs in magnitude of the response slightly at the high end of the frequency range, but phase agreement is good throughout the range. Overall, the longitudinal model is suitable for flight control development.

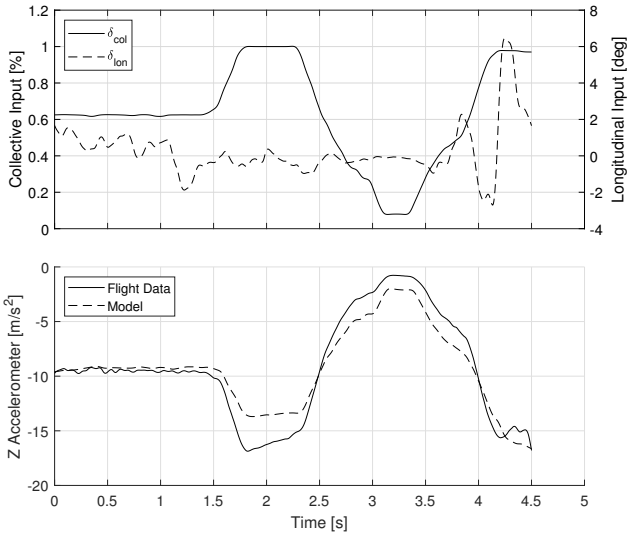

Fig. 5 Longitudinal model verification in time domain using a collective input

B. Lateral-Directional Model

The lateral-directional model is identified using the frequency response pairs and ranges shown in Table 6. The high frequency range of the p/δ_{lat} response represents the fast roll response of the light quad-rotor. No cross-coupling from the longitudinal inputs to the lateral motion was observed so those frequency responses are not included. The identified model results in individual and average cost functions which are well below $J = 100$ and indicate excellent agreement between the model and frequency responses.

Similar to the longitudinal model, the speed-damping derivative Y_v is identified using a transfer function fit to $\dot{v}/\phi(s)$ Eq. (5). This achieves a good identification of this parameter, which is important for a hovering model, while avoiding the typical issues of poor coherence in the low frequency ranges. A frequency range of 1.5-12 rad/s was chosen based on the coherence in the flight data. The resulting value of Y_v is identified as -0.18.

$$\dot{v}/\phi(s) = \frac{sg}{s - Y_v} \tag{5}$$

The resulting model parameters are shown in Table 7. The L_p, N_v, and Y_r parameters are dropped from both models due to high insensitivity or high Cramér-Rao bounds. The control parameters $L_{\delta_{ped}}$, and $Y_{\delta_{ped}}$ were eliminated in the model structure (before identification) due to the lack of cross-coupling observed in the data. All remaining parameters except L_r and N_p have acceptable Cramér-Rao bounds and insensitivities. The L_r and N_p parameters were retained in the model despite their higher insensitivity and Cramér-Rao values in order to prevent the cost function from rising

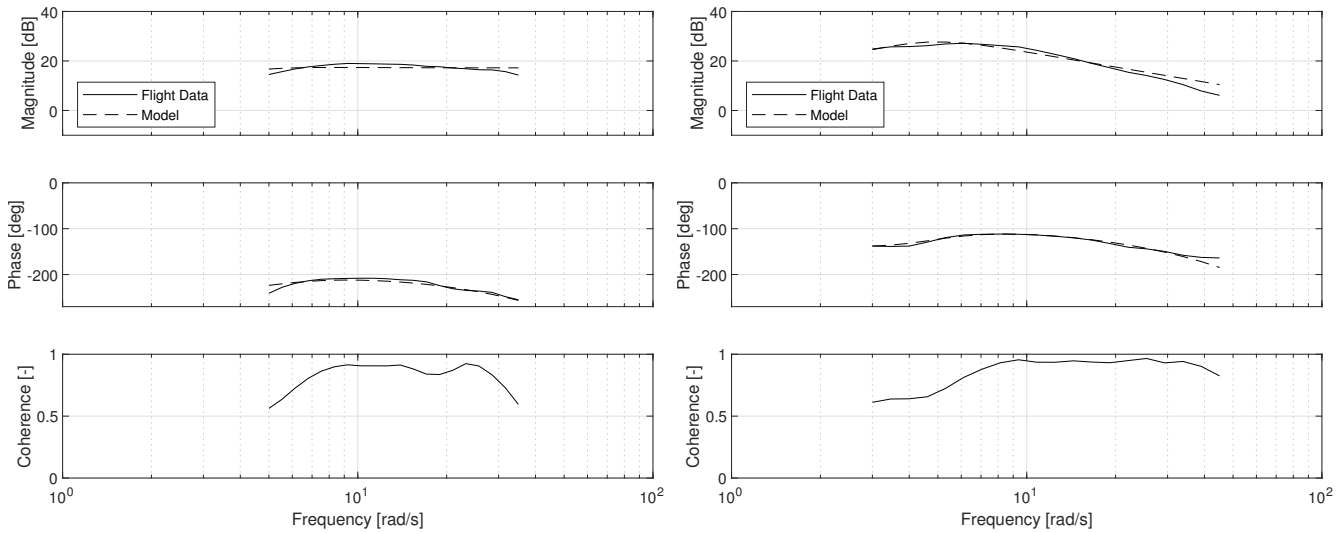

(a) A_x/δ_{lon} frequency response verification

(b) q/δ_{lon} frequency response verification

Fig. 6 Longitudinal model verification in frequency domain

Table 6 Lat-dir model frequency range and cost functions

Response	ω_{min} [rad/s]	ω_{max} [rad/s]	J [-]
p/δ_{lat}	4.5	30	25.7
r/δ_{lat}	9.6	20	22.9
ϕ/δ_{lat}	5	13	7.3
$\dot{v}/\delta_{lat}$	4	28	19.9
A_y/δ_{lat}	5	27	27.0
r/δ_{ped}	1	21	96.8
J_{avg} [-]			49.9

excessively. The lateral time delay shows good agreement with the longitudinal model, which is appropriate given the same motor response causes the delay in the lateral axis as well as the longitudinal.

The resulting eigenvalues of the lat-dir model are shown in Table 8 and reveal two oscillatory modes, one stable and one unstable. The stable mode is nearly first order with a high damping ratio of 0.99. The unstable mode is typical of rotorcraft in hovering flight.

Verification of the lat-dir stable mode is accomplished with a rudder doublet in and the results are shown in Fig. 8. The model tracks the input from the flight data very well throughout the maneuver with minor differences in the magnitude of the response. Verification of the unstable modes is provided in a frequency domain comparison between the model and the flight data in Fig. 9 and 10. The roll and bank angle response in Fig. 9 shows excellent agreement in magnitude and phase of the model response compared to the flight data. The side acceleration and velocity in Fig. 10 also shows excellent agreement in magnitude and phase throughout the frequency range.

Table 7 Identified lat-dir model parameters

Parameter	Value	Cramér-Rao [%]	Insensitivity [%]
L_p [1/s]	-	-	-
L_r [1/s]	-21.6	51.2	15.4
L_v [1/s]	-6.7	13.8	6.3
N_p [1/s]	0.06	42.1	16.6
N_r [1/s]	-3.8	9.3	2.9
N_v [1/s]	-	-	-
Y_p [1/s]	0.11	16.4	7.0
Y_r [1/s]	-	-	-
Y_v [1/s]	-0.18	-	-
$L_{\delta_{lat}}$ [1/s^2]	153.4	2.8	0.9
$N_{\delta_{lat}}$ [1/s^2]	-4.0	5.6	2.7
$Y_{\delta_{lat}}$ [1/s^2]	7.4	3.4	1.4
$N_{\delta_{ped}}$ [1/s^2]	31.1	5.9	2.0
$\tau_{\delta_{lat}}$ [s]	0.041	4.9	1.9
$\tau_{\delta_{ped}}$ [s]	-	-	-

Table 8 Lat-dir eigenvalues of the S500 quad-rotor

Mode	Real	Imaginary	ζ [-]	ω_n [rad/s]
1	-3.88	± 0.62	0.99	3.9
2	1.87	± 3.58	-0.46	4.0

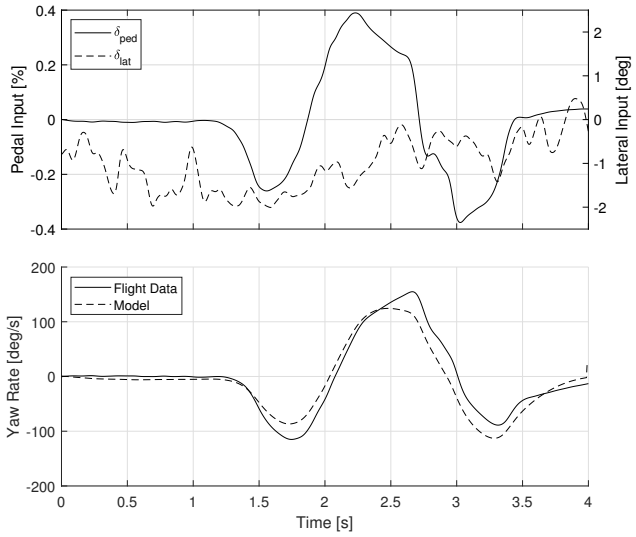

Fig. 7 Lateral-directional model verification using a pedal input

V. Conclusion

Flight tests were performed on a kit-built S500 quad-rotor aircraft to obtain frequency sweeps in the manual (stabilize) autopilot mode. The flight controller output was used to identify the bare-airframe vehicle dynamics, both

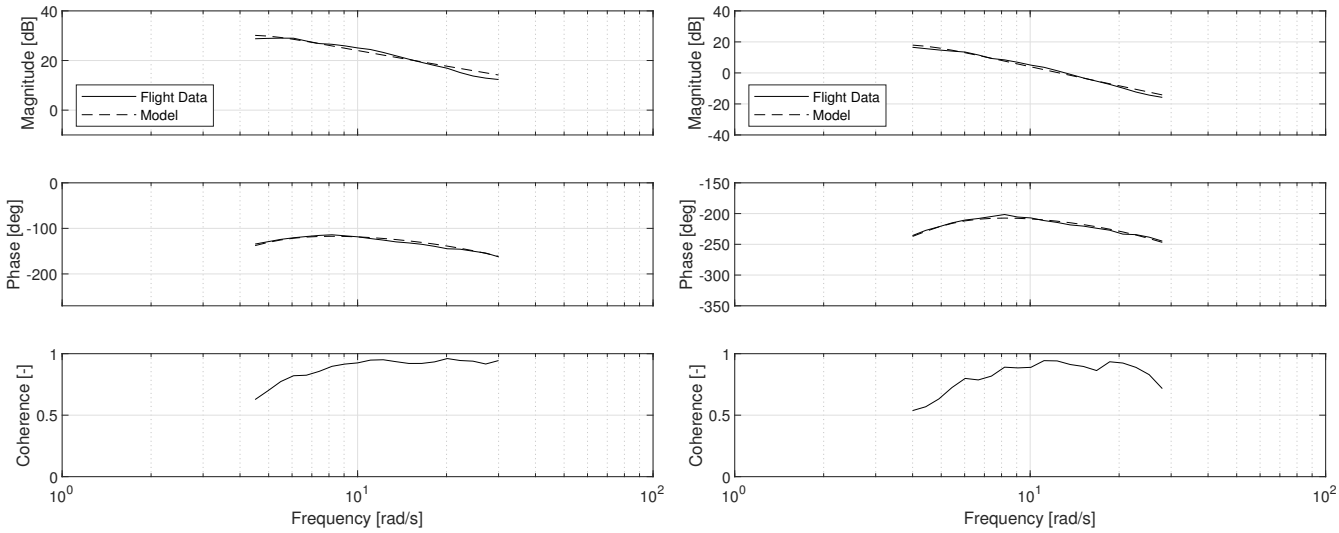

(a) p/δ_{lat} frequency response verification

(b) ϕ/δ_{lat} frequency response verification

Fig. 8 Lat-dir model verification in frequency domain

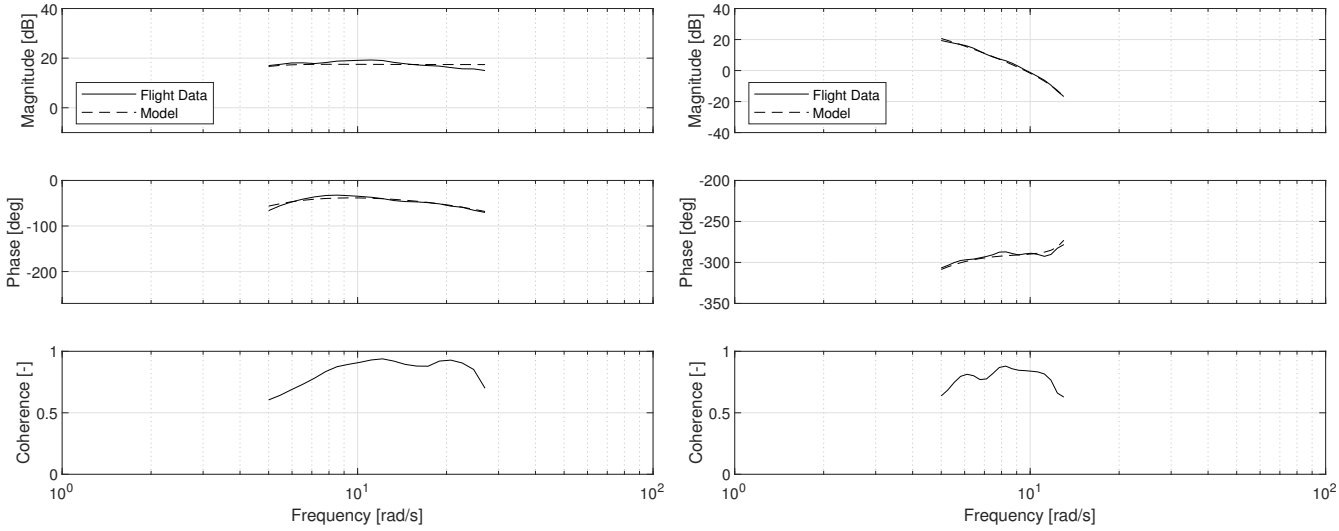

(a) A_y/δ_{lat} frequency response verification

(b) v/δ_{lat} frequency response verification

Fig. 9 Lat-dir model verification in frequency domain

longitudinal and lateral-directional, using system identification in the frequency domain.

In the longitudinal case, the model was valid over a frequency range from 1 to 45 rad/s with two stable, real eigenvalues and one pair of unstable eigenvalues corresponding to the classic unstable hovering dynamic associated with rotorcraft. The verification in the time and frequency domains showed the accuracy of the model.

In the lateral-directional case, a similar frequency range from 1-30 rad/s was achieved with one stable oscillatory mode and one unstable oscillatory mode. The model response in the frequency and time domain was acceptable when compared to flight data.

In both models, the speed damping derivative was identified from a separate transfer function procedure and inserted into the model manually. Unnecessary parameters were dropped while some parameters which slightly violated the insensivity and Cramér-Rao rules-of-thumb were retained for the sake of the overall cost function. Time delays across both models were close to 40 milliseconds which is characteristic of the quad-rotor motors in use.

Overall, these two models form a complete 6DOF prediction of the vehicle dynamics in hovering flight.The models show excellent predictive agreement to flight data and are suitable for further control law design for the S500.

Acknowledgments

The author would like to thank the Edison Grant program of the U.S. Air Force for supporting this work.

References

[1] Smith, G. D., Bixler, B. M., Babcock, J. T., Osteroos, R. K., McLaughlin, T. E., and Tischler, M. B., "System Identification of the ICE/SACCON UAS Aircraft," *AIAA Paper 2020-0289*, 2020. https://doi.org/10.2514/6.2020-0289.

[2] Knapp, M. E., Berger, T., Tischler, M., and Cotting, M. C., "Development of a Full Envelope Flight Identified F-16 Simulation Model," *AIAA Paper 2018-0525*, 2018, pp. 1–28. https://doi.org/10.2514/6.2018-0525.

[3] Lederbogen, P., Colgren, R., and Kowalchuk, S., "Model Generation and Performance with CIFER," *AIAA Paper 2005-6424*, 2005. https://doi.org/10.2514/6.2005-6424.

[4] Cho, S. H., Bhandari, S., Sanders, F. C., Cheung, K. K., and Tischler, M. B., "System Identification and Controller Optimization of a Coaxial Quadrotor UAV in Hover," *AIAA Paper 2019-1075*, 2019, pp. 1–15. https://doi.org/10.2514/6.2019-1075.

[5] Tischler, M. B., and Remple, R. K., *Aircraft and Rotorcraft System Identification*, 2nd ed., 2012.

[6] Mettler, B., Tischler, M. B., and Kanade, T., "System Identification of Small-Size Unmanned Helicopter Dynamics," *Annual Forum Proceedings - American Helicopter Society*, Vol. 2, 1999, pp. 1706–1717.

[7] Cai, G., Al Mehairi, H., Al-Hosani, H., Dias, J., and Seneviratne, L., "Frequency-Domain Flight Dynamics Model Identification of MAVs - Miniature Quad-Rotor Aerial Vehicles," *IEEE International Conference on Intelligent Robots and Systems*, , No. Iros, 2014, pp. 3376–3381. https://doi.org/10.1109/IROS.2014.6943032.

[8] Wei, W., Tischler, M. B., Schwartz, N., and Cohen, K., "Frequency-Domain System Identification and Simulation of a Quadrotor Controller," , No. January, 2011. https://doi.org/10.1007/978-94-007-0023-9_5.

[9] Niermeyer, P., Raffer, T., and Holzapfel, F., "Open-Loop quadrotor flight dynamics identification in frequency domain via Closed-Loop flight testing," *AIAA Guidance, Navigation, and Control Conference, 2013*, , No. January, 2015. https://doi.org/10.2514/6.2015-1539.

[10] Navarro, P., Cho, S., Rashid, A., Ruiz, A., and Bhandari, S., "Flight testing, data collection, and system identification of a multicopter UAV," *AIAA Modeling and Simulation Technologies Conference, 2017*, , No. January, 2017, pp. 1–15. https://doi.org/10.2514/6.2017-1558.

[11] Cheung, K. K., Wagster, J. A., Tischler, M. B., Ivler, C. M., Berrios, M. G., Berger, T., Juhasz, O., Tobias, E. L., Goerzen, C. L., Barone, P. S., Sanders, F. C., Lopez, M. J., and Lehmann, R. M., "An overview of the U.S. Army aviation development directorate quadrotor guidance, navigation, and control project," *Annual Forum Proceedings - AHS International*, , No. May, 2017, pp. 2894–2912.

[12] Yuksek, B., Saldiran, E., Cetin, A., Yeniceri, R., and Inalhan, G., "System Identification and Model-Based Flight Control System Design for an Agile Maneuvering Quadrotor Platform," *AIAA Scitech 2020 Forum*, Vol. 1 PartF, No. January, 2020, pp. 1–25. https://doi.org/10.2514/6.2020-1835.